

**UNCLASSIFIED**

NAVAL AIR WARFARE CENTER AIRCRAFT DIVISION  
PATUXENT RIVER, MARYLAND



## **TECHNICAL REPORT**

REPORT NO: NAWCADPAX/TR-2007/11

### **FATIGUE OF Ti-3Al-2.5V ALLOY TUBE AND ROD**

by

**E. U. Lee  
R. E. Taylor  
H. C. Sanders  
C. Lei  
M. Yu**

**28 February 2007**

Approved for public release; distribution is unlimited.

**UNCLASSIFIED**

DEPARTMENT OF THE NAVY  
NAVAL AIR WARFARE CENTER AIRCRAFT DIVISION  
PATUXENT RIVER, MARYLAND

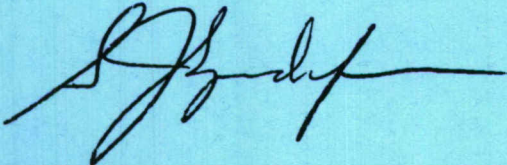
NAWCADPAX/TR-2007/11  
28 February 2007

FATIGUE OF Ti-3Al-2.5V ALLOY TUBE AND ROD

by

E. U. Lee  
R. E. Taylor  
H. C. Sanders  
C. Lei  
M. Yu

**RELEASED BY:**

 28Feb07

---

STEPHEN SPADAFORA / AIR-4.3.4 / DATE  
Division Head, Materials Engineering Division  
Naval Air Systems Command

REPORT DOCUMENTATION PAGE			Form Approved OMB No. 0704-0188		
Public reporting burden for this collection of information is estimated to average 1 hour per response, including the time for reviewing instructions, searching existing data sources, gathering and maintaining the data needed, and completing and reviewing this collection of information. Send comments regarding this burden estimate or any other aspect of this collection of information, including suggestions for reducing this burden, to Department of Defense, Washington Headquarters Services, Directorate for Information Operations and Reports (0704-0188), 1215 Jefferson Davis Highway, Suite 1204, Arlington, VA 22202-4302. Respondents should be aware that notwithstanding any other provision of law, no person shall be subject to any penalty for failing to comply with a collection of information if it does not display a currently valid OMB control number. PLEASE DO NOT RETURN YOUR FORM TO THE ABOVE ADDRESS.					
1. REPORT DATE 28 February 2007		2. REPORT TYPE Technical Report		3. DATES COVERED	
4. TITLE AND SUBTITLE  Fatigue of Ti-3Al-2.5V Alloy Tube and Rod			5a. CONTRACT NUMBER		
			5b. GRANT NUMBER		
			5c. PROGRAM ELEMENT NUMBER		
6. AUTHOR(S)  E. U. Lee R. E. Taylor H. C. Sanders C. Lei M. Yu			5d. PROJECT NUMBER		
			5e. TASK NUMBER		
			5f. WORK UNIT NUMBER		
7. PERFORMING ORGANIZATION NAME(S) AND ADDRESS(ES)  Naval Air Warfare Center Aircraft Division 22347 Cedar Point Road, Unit #6 Patuxent River, Maryland 20670			8. PERFORMING ORGANIZATION REPORT NUMBER  NAWCADPAX/TR-2007/11		
9. SPONSORING/MONITORING AGENCY NAME(S) AND ADDRESS(ES)  Naval Air Systems Command 47123 Buse Road, Unit IPT, Bldg. 2272 Patuxent River, Maryland 20670-1906			10. SPONSOR/MONITOR'S ACRONYM(S)		
			11. SPONSOR/MONITOR'S REPORT NUMBER(S)		
12. DISTRIBUTION/AVAILABILITY STATEMENT  Approved for public release; distribution is unlimited.					
13. SUPPLEMENTARY NOTES					
14. ABSTRACT  The hydraulic impulse fatigue of Ti-3Al-2.5V alloy tube was studied under cyclic hydraulic pressurization and the low cycle fatigue (LCF) of the alloy tube and rod under cyclic axial straining. Employing a newly fabricated test frame, the cyclic-pressurization-induced fatigue crack growth through the tube wall thickness was characterized quantitatively. On the basis of the results, a relationship between electric potential drop and crack depth was established and a method of determining fatigue crack initiation, growth, and fracture lives was also defined. The LCF behavior of the alloy tube and rod was investigated, examining the shape change of load-displacement hysteresis loop and the drop of load and elastic modulus with increasing strain-cycle. The LCF crack initiation and growth lives were defined. They were found to follow the Coffin-Manson relation with relatively longer LCF crack initiation life. The LCF lives were longer for the tube than the rod. This is attributable to the greater cold work done in the tube forming process, evidenced by the smaller grain size and higher tensile strength.					
15. SUBJECT TERMS  High Cycle Fatigue (HCF), Low Cycle Fatigue (LCF), Cyclic Hydraulic Pressurization, Electric Potential Drop, Hysteresis Loop, Elastic Modulus, Crack Initiation and Growth, Cold Work, Work-Hardening, Work-Softening, Strain-Cycle					
16. SECURITY CLASSIFICATION OF:			17. LIMITATION OF ABSTRACT	18. NUMBER OF PAGES	19a. NAME OF RESPONSIBLE PERSON
a. REPORT	b. ABSTRACT	c. THIS PAGE			E. U. Lee
Unclassified	Unclassified	Unclassified	SAR	39	19b. TELEPHONE NUMBER (include area code) (301) 342-8069

## SUMMARY

A new test frame was fabricated to conduct cyclic pressurization (or hydraulic impulse fatigue) test of Ti-3Al-2.5V alloy tube. With this frame, the fatigue crack growth through the wall thickness of a tube was monitored by means of electric potential drop, and a method was established to determine the fatigue crack initiation, growth, and fracture lives.

The Ti-3Al-2.5V alloy tube and rod were subjected to cyclic straining, and their low cycle fatigue (LCF) behaviors were studied and compared. It was observed that the shape of load-displacement hysteresis loop was changed, and the load and elastic modulus were reduced with increasing strain-cycle. On the basis of this observation, the criteria for LCF crack initiation and growth lives were defined.

Most of the LCF life was consumed for fatigue crack initiation, resulting in a shorter fatigue crack growth life. The LCF life was also found to be longer for the tube than the rod, resulting from the greater cold work, smaller alpha grain, and higher tensile strength of the tube. Furthermore, it was confirmed that the Coffin-Manson relationship is applicable to the LCF initiation, 50% load drop, and fracture of the alloy tube and rod.

Contents

	<u>Page No.</u>
Summary .....	ii
Acknowledgement .....	iv
Introduction.....	1
Experimental Procedures .....	2
Specimen.....	2
Tension Test.....	3
Hydraulic Impulse Fatigue Test.....	4
Low Cycle Fatigue Test.....	4
Results and Discussion .....	4
Micrograph.....	4
Mechanical Properties.....	5
Crack Growth during Hydraulic Impulse Fatigue .....	5
Load-Displacement Hysteresis Loop.....	5
Strain-Life Curve .....	7
Conclusions.....	9
References.....	10
Appendix	
A. Figures .....	11
Distribution .....	32

## ACKNOWLEDGEMENT

The support of this work from the V-22 program is gratefully acknowledged. The authors also wish to thank Mr. Elmer W. Stone (former V-22 Development Deputy, Logistics), Mr. Thomas Speidel (MV-22 Development IPT), and Mr. Michael D. Poliszuk (MV-22 Deputy Class Desk) for their guidance and interest.

## INTRODUCTION

Ti-3Al-2.5V alloy is a near alpha, alpha-beta alloy, sometimes referred to as “half-6-4.” It offers 20 to 50% higher tensile strength than the commercially pure titanium at room and elevated temperatures. It is much more amenable to cold working than Ti-6Al-4V alloy and can be cold worked 75 to 85% to result in moderately high strength and good ductility. Furthermore, it is weldable as the commercially pure grades and has excellent resistance to torsion and corrosion. Therefore, it is used principally as tubing in aircraft hydraulic systems and as foil in aircraft honeycomb panels. Its non-aerospace applications include sport equipments, medical and dental implants, and ballpoint-pen casings.

Ti-3Al-2.5V alloy seamless tubing was originally developed for aircraft hydraulic and fuel systems. The Lockheed C-5A was the first military aircraft in which Ti-3Al-2.5V alloy tubing was employed. This tubing was also selected for the hydraulic system of the Concord Supersonic Transport. Its first application in subsonic commercial aircraft was the Boeing 767. Since then, this alloy tubing has been chosen for most of the other commercial transports, commuter aircraft, and spacecraft.

The reliability of tubing is adversely affected by cracking in service, resulting from internal and surface irregularities. Production defects may be inclusions, separations in the tubing wall, or fissures at the inner and outer surfaces. Surface damage usually takes the form of chafing or denting. Recently, Ti-3Al-2.5V alloy tubing has been observed to fail under cyclic hydraulic pressurization or hydraulic impulse fatigue and strain cycling.

In an end-capped tubing with internal pressure, the induced circumferential or hoop stress is known to be twice the axial stress. Therefore, it is highly likely that an axial (or longitudinal) surface crack is initiated normal to the circumferential stress under cyclic pressurization or hydraulic impulse fatigue in a hydraulic tubing. Subsequently, hydraulic oil leaks out of the tubing, resulting in lower oil pressure, malfunction of hydraulic system, and also fire. However, the hydraulic impulse fatigue crack initiation and growth have not been fully characterized, and their lives have not been correctly estimated.

Although most engineering structures and components are designed such that the nominal loads remain elastic, stress concentrations often cause plastic strain to develop in the vicinity of notches. Due to the constraint imposed by the elastically stressed material surrounding the plastic zone, deformation at the notch root is considered strain-controlled. The strain-life or low cycle fatigue (LCF) method assumes that smooth specimens tested under strain-controlled can simulate fatigue damage at the notch root of an engineering component. Equivalent fatigue damage and life are assumed to occur at the notch root and in the smooth specimen when both are subjected to identical stress-strain histories (reference 1). Thus, for the clarification of tubing reliability, it is essential to investigate the LCF behavior of tubing and rod of Ti-3Al-2.5V alloy.

Several alternative LCF failure criteria have been proposed in the literature (references 1 through 6). Some of them are total separation or fracture of the specimen into two parts, a predetermined load or elastic modulus drop from the peak value, and shape change of hysteresis loop and/or formation of a cusp in its compressive portion. Rao et al (reference 3) conducted LCF test of 304 stainless steel and defined the inflection point in the plot of elastic modulus versus number of strain cycles as the microcrack initiation life. During their high-temperature LCF testing of Rene 80, Romanoski et al (reference 4) observed a sudden decay in the maximum load with appearance and onset of propagation of one or more cracks and defined it as the LCF failure. Raske and Morrow (reference 5) found a cusp in the hysteresis loop during cyclic straining of a 18% nickel maraging steel and attributed it to the presence of a crack. Skelton (reference 6) also attributed a hysteresis loop cusp to the presence of a crack in a ½ Cr-Mo-V steel. Frost et al (reference 7) noticed an association of hysteresis loop width change with crack growth.

This study was conducted to clarify the characteristics of Ti-3Al-2.5V alloy tubing failure, including crack initiation and growth, induced by hydraulic impulse fatigue and low cycle fatigue, and to establish the valid ways of service life prediction and failure prevention or mitigation.

## EXPERIMENTAL PROCEDURES

### SPECIMEN

Two kinds of Ti-3Al-2.5V alloy specimens, tube and rod, were employed. These materials were initially subjected to the following heat treatments and their chemical compositions are shown in table 1.

#### Tube

- Solution Treatment: ¼ hr at 871°C (1600°F) and water quenching
- Aging: 2 hr at 482°C (900°F) and vacuum cooling
- Cold Work for Tube Fabrication
- Stress Relief: ½ hr at 371°C (700°F)

#### Rod

- Solution Treatment: 1 hr at 927°C (1700°F) and water quenching
- Aging: 6 hr at 482°C (900°F) and air cooling



Table 1: Chemical Compositions of Tube and Rod of Ti-3Al-2.5V Alloy (Weight %)

Element	Tube	Rod
Al	3.000	2.97
B	<0.0005	
C	0.005	0.01
Cu	<0.002	
Fe	0.151	0.13
H	0.0014	60 ppm
Mn	0.001	
N	0.003	<0.01
O	0.093	0.11
Si	0.005	
Ti	Balance	Balance
V	2.520	2.23
W	<0.003	

The specimens are shown in figures A-1 and A-2 and their dimensions are as follows:

#### Tube

Tube Tension and LCF Test Specimen: The outside diameter (OD) is 3/8 in., the wall thickness 0.032 in., the gage length 0.300 in., and the length 2.92 in. The ends of the tube were pressed into a PHENOLIC bushing, 1.00 in. long and 0.750 in. diameter. The bushings were used to keep the tubes from fatiguing at the metal collet interface on the hydraulic grips. DELRIN inserts were pressed inside the tube to keep it from deforming due to the hydraulic pressure.

Hydraulic Impulse Fatigue Test Specimen: The OD is 3/8 in., the thickness 0.032 in., and the length 8 in. This specimen has an axial Laser notch, 0.07 in. long and 0.005 in. deep, and wiring for electric potential drop (PD) measurement on its OD surface.

#### Rod

Tension and LCF Test Specimen: The diameter is 1/4 in., the gage length 1/2 in., and the length 3.3 in.

#### TENSION TEST

Employing a LCF test specimen with an extensometer of 0.010 in. range mounted, the tension tests for the tube and rod specimens were conducted, following ASTM E8, Standard Test Methods for Tension Testing of Metallic Materials (reference 8), at room temperature in laboratory air. The loading rate was 0.01 in./min.

### HYDRAULIC IMPULSE FATIGUE TEST

For the hydraulic impulse fatigue test, a test frame was fabricated and a direct current (DC) PD measurement system was assembled.

The hydraulic test frame consists of a MTS 3000 psi hydraulic pump, a MTS hydraulic pressure manifold with servovalve, a hydraulic pressure intensifier, 1000 psi pressure transmitter, and a specimen-holder, figure A-3. The frame is controlled by a MTS 458 controller.

The DC PD measurement system consists of a 0-20 amp HP power supply, solid state switching relays, and VISHAY 2310 signal amplifiers. The current leads were spot-welded on the tube at the 0 deg and 180 deg position above and below the Laser notch. The readout leads were spot-welded 50 mils above and below the notch.

The test frame and DC PD measurement system are interfaced with a FTA fatigue crack growth computer system, which monitors the cyclically changing hydraulic oil pressure and PD in a specimen tube and processes the data being generated.

The hydraulic impulse fatigue test was performed by cyclically pressurizing the specimen tube, following the pressure waveform of SAE ARP 603 with maximum pressure 7500 psi, minimum pressure 75 psi, and an intermediate plateau of 5000 psi, figure A-4. The pressurization frequency was 1 Hz, and the DC PD was measured at various pressurization cycles. After the hydraulic impulse fatigue test, the specimen tube was heated (or heat-tinted) at 566°C (1050°F) for 2 hr in air to oxidize the newly generated crack surfaces. The specimens were broken open to measure the crack surface, which was oxidized or discolored. Subsequently, a calibration curve of DC PD versus crack depth was prepared.

### LOW CYCLE FATIGUE TEST

Employing a LCF test specimen with an extensometer of 0.010 in. range mounted, the LCF test was performed in a MTS machine of 20 kip (89 KN) capacity under strain-control. The cyclic straining was done in axial or longitudinal orientation at frequencies, 5 Hz for the rod specimen, 1 Hz for lower strain amplitudes, and 0.33 Hz for higher strain amplitudes, to reduce the specimen heating for the tube specimen. The strain waveform was triangular, its ratio -1, and the test environment laboratory air at ambient temperature.

## RESULTS AND DISCUSSION

### MICROGRAPH

For both of the tube and rod specimens, the micrographs of the longitudinal face showed elongated light alpha grains and that of the cross-section equiaxed light alpha grains with small amount of dark beta along grain boundaries, figure A-5. The diameters of the equiaxed alpha grains were 4 µm and 5 µm for the tube and rod specimens, respectively.

MECHANICAL PROPERTIES

The mechanical properties in the longitudinal orientation were determined to be:

	Tube	Rod
Tensile Yield Strength (MPa)	745 (108 ksi)	621 (90 ksi)
Ultimate Tensile Strength (MPa)	883 (128 ksi)	745 (108 ksi)
Tensile Elongation (%)	15	21

CRACK GROWTH DURING HYDRAULIC IMPULSE FATIGUE

After hydraulic impulse fatigue test for a given number of pressurization cycles and heat-tinting, the crack in a tube specimen was opened up. Such crack surfaces are shown in figure A-6. The gray area along the tube OD surface is Laser notch and the blue area the heat-tinted area of crack growth. The blue (tinted) area grew larger with increasing pressurization cycle and eventually penetrated through the tube wall.

With the measured PD and crack depth, two calibration curves were plotted. One is the plot of normalized PD  $[(V/V_o) - 1]$  versus crack depth  $a$ , figure A-7, and the other the plot of normalized PD versus normalized crack depth  $a/B$ , where  $B$  is the tube wall thickness, figure A-8. The linear relationship on log-log coordinates can be expressed by the following equations.

$$[(V/V_o) - 1] = 2398(a)^{2.79} \quad (1)$$

$$[(V/V_o) - 1] = 0.16(a/B)^{2.80} \quad (2)$$

From these plots or equations, a crack depth  $a$  or normalized one  $a/B$  can be found for a PD measured at a given pressurization cycle.

LOAD-DISPLACEMENT HYSTERESIS LOOP

A load-displacement hysteresis loop (hereafter referred to as "hysteresis loop") is formed by one cycle of straining and reflects the LCF behavior of a specimen at a given number of strain-cycles. A stable hysteresis loop, shown in figure A-9, indicates elastic ( $\Delta\epsilon_e$ ), plastic ( $\Delta\epsilon_p$ ), and total ( $\Delta\epsilon$ ) strain ranges; elastic moduli  $E$  in tension and compression; and maximum stress  $\sigma_{max}$ , minimum stress  $\sigma_{min}$ , and total stress range  $\Delta\sigma$ . The elastic modulus is the slope of the straight line of unloading from the peak tensile stress or that of loading from the peak compression stress.

During cyclic straining, the shape of a hysteresis loop is changed by work softening and/or hardening and load drop and elastic modulus change, arising from crack initiation and growth. An example of such a change is shown in figure A-10. With an increasing number of strain-cycle, the height, depth, and width of the hysteresis loop and the slopes of its straight portions change, and so the overall loop shape changes, eventually forming a cusp, figures A-10 and

A-11. In other words, the peak tensile and compressive stresses, elastic and plastic strain ranges, elastic moduli in tension and compression ( $E_{NT}$  and  $E_{NC}$ ), and their ratio  $Q_N = E_{NT}/E_{NC}$  change with cyclic straining, figure A-11.

There have been four conventional definitions of LCF failure, employed by many investigators (reference 3). They are Separation of Specimen: that is, total separation or fracture of a specimen into two parts, Modulus Ratio 0.5, 50% Load (or Stress) Drop, and Shape Change of Hysteresis Loop. However, none of these definitions can identify a fatigue crack initiation or its life. Therefore, an attempt was made to find the fatigue crack initiation life in this investigation. It has been observed that the tensile load drops at the end of stable cyclic straining. The inception or the very beginning of such a load drop is believed to be associated with the fatigue crack initiation and indicates its life. When load is plotted against strain-cycle, the maximum tensile load drop is evidenced by a deviation of the tensile curve at the end of stable cyclic straining, figure A-12. In this investigation, the particular strain-cycle for the tensile curve deviation (inflection) is defined as the fatigue crack initiation life  $N_i$ . In addition, the strain-cycle, at which the maximum tensile load drops to 50% of the initial one, is defined as 50% load drop fatigue life  $N_{50}$ . This is equal to the fatigue crack initiation life  $N_i$  plus the fatigue crack growth life to 50% load drop. In the LCF test of a tube specimen, it is difficult to detect the clear separation of a specimen. Therefore, the fatigue fracture life cannot be determined accurately and it is not used as a measure of LCF failure of tube specimen in this investigation. On the other hand, the fatigue fracture life is correctly measurable for a round rod specimen. When the modulus ratio  $Q_N$  is plotted against strain-cycle  $N$ , there is also a curve deviation (inflection) at the end of stable cyclic straining, figure A-13. The particular strain-cycle for this curve deviation is found to be similar to that for the plot of load versus strain-cycle, the fatigue crack initiation life  $N_i$ . In other words, the fatigue crack initiation life  $N_i$  can be found from either plot of load versus strain-cycle or that of modulus ratio versus strain-cycle. To verify the fatigue crack initiation, a tube specimen was heat-tinted at 538°C (1,000°F) after cyclic straining for a period, slightly longer than the  $N_i$ , and opened up the crack. The fracture surface shows two small discolored thumbnail-shape cracks along the OD surface, figure A-14. This observation indicates that the larger crack was initiated first on the OD surface at or near the fatigue crack initiation life. On the basis of this observation, the following definition of LCF failure is adopted in this investigation:

- Fatigue Crack Initiation Life  $N_i$ : Number of Strain-Cycles for Inception of Maximum Tensile Load Drop (or Deviation of Load versus Strain-Cycle Curve from Stable Line)
- 50% Load Drop Fatigue Life  $N_{50}$ : Number of Strain-Cycles to 50% Load Drop =  $N_i$  + Fatigue Crack Growth Life to 50% Load Drop
- Fatigue Fracture Life  $N_f$ : Number of Strain-Cycles for Separation or Fracture of Specimen

STRAIN-LIFE CURVE

Figure A-15 shows a strain-life curve, elastic and plastic strain lines, their intercepts and slopes, and hysteresis loops at different strain-cycles. Such a curve can be expressed with the Coffin-Manson equation (references 9 and 10).

$$\Delta\varepsilon/2 = (\Delta\varepsilon_e/2) + (\Delta\varepsilon_p/2) = (\sigma_f'/E)(2N)^b + \varepsilon_f'(2N)^c \quad (3)$$

where

$\Delta\varepsilon/2$  = total strain amplitude

$\Delta\varepsilon_e/2$  = elastic strain amplitude =  $\Delta\sigma/2E$

$\Delta\varepsilon_p/2$  = plastic strain amplitude =  $(\Delta\varepsilon/2) - (\Delta\varepsilon_e/2)$

$\Delta\sigma/2$  = stress amplitude

$E$  = modulus of elasticity

$\sigma_f'$  = fatigue strength coefficient

$N$  = number of strain-cycles

$b$  = fatigue strength exponent

$\varepsilon_f'$  = fatigue ductility coefficient

$c$  = fatigue ductility exponent

If only the plastic strain-life is considered,

$$\Delta\varepsilon_p/2 = \varepsilon_f'(2N)^c \quad (4)$$

TUBE SPECIMEN

The strain-life curves of strain amplitude,  $\Delta\varepsilon_p/2$ , versus strain reversal,  $2N_i$  or  $2N_{50}$ , for fatigue crack initiation and 50% load drop in tube specimens are shown in figure A-16. The linear relationship on log-log coordinates can be expressed by the following equations:

$$\Delta\varepsilon_p/2 = (8.95 \times 10^{-2})(2N_i)^{-0.262} \quad (5)$$

$$\Delta\varepsilon_p/2 = (3.21 \times 10^{-1})(2N_{50})^{-0.400} \quad (6)$$

The two curves nearly overlap each other, indicating that most of the fatigue life was consumed for crack initiation.

## ROD SPECIMEN

The strain-life curves of strain amplitude,  $\Delta\varepsilon_p/2$ , versus strain reversal,  $2N_i$ ,  $2N_{50}$ , and  $2N_f$ , for fatigue crack initiation, 50% load drop, and fracture in rod specimens are shown in figure A-17, and they can be expressed by the following equations:

$$\Delta\varepsilon_p/2 = (3.90 \times 10^{-2})(2N_i)^{-0.185} \quad (7)$$

$$\Delta\varepsilon_p/2 = (4.37 \times 10^{-2})(2N_{50})^{-0.195} \quad (8)$$

$$\Delta\varepsilon_p/2 = (4.57 \times 10^{-2})(2N_f)^{-0.200} \quad (9)$$

The three curves also nearly overlap each other, indicating the long fatigue crack initiation life and the short fatigue crack propagation life.

Figures A-16 and A-17 and the corresponding equations (5) through (9) evidence the applicability of the Coffin-Manson relationship (references 9 and 10) to the fatigue crack initiation and 50% load drop in the tube and rod of Ti-3Al-2.5V alloy, as well as to the fatigue fracture in the rod.

The strain-life curves of tube and rod specimens for fatigue crack initiation are compared in figure A-18 and those for fatigue 50% load drop in figure A-19. Those curves indicate that the tube specimen has longer fatigue crack initiation and 50% load drop lives than the rod specimen. This is attributable to the greater cold work, evidenced by smaller alpha grain and higher tensile strength of the tube specimen. Furthermore, this must also be associated with the different textures of the tube and rod, arising from their different forming processes.

## CONCLUSIONS

- The criteria for the initiation and growth life of the LCF crack in the Ti-3Al-2.5V alloy tube and rod are definable from the shape change of load-displacement hysteresis loop.
- The LCF life is longer for the tube than the rod. This is attributed to the greater cold work, smaller alpha grain, and higher tensile strength of the tube.
- The Coffin-Manson relationship is applicable to the LCF initiation and fracture lives of the tube and rod.

REFERENCES

1. Julie A. Bannantine, Jess J. Comer, and James L. Handrock, "Fundamentals of Metal Fatigue Analysis," Prentice Hall Inc., Englewood Cliffs, NJ, 1990, p. 40.
2. Designation: E606-92, 1996 Annual Book of ASTM Standards, 03.01, ASTM International, West Conshohocken, PA, 2003.
3. K. B. S. Rao, M. Valsan, R. Sandhya, and S. K. Ray, S. L. Mannan, and P. Rodriguez, *Int J Fatigue*, 141, 1985.
4. G. R. Romanoski, S. D. Antolovich, and R. M. Pelloux, *Low Cycle Fatigue*, ASTM STP 942, American Society for Testing and Materials, 456, 1988.
5. D. T. Raske and J. D. Morrow, *Manual on Low Cycle Fatigue Testing*, ASTM STP 465, American Society for Testing and Materials, 1, 1969.
6. R. P. Skelton, *Low Cycle Fatigue*, ASTM STP 942, American Society for Testing and Materials, 209, 1988.
7. N. E. Frost, K. L. Marsh, L. P. Pook, *Metal Fatigue*, Clarendon Press, Oxford, 17, 1974.
8. Designation: E8-01, 2003 Annual Book of ASTM Standards, 03.01, ASTM International, West Conshohocken, PA, 2003.
9. L. F. Coffin, *Trans ASME*, 76, 931, 1954.
10. S. S. Manson, on *National Advisory Commission Aeronautics: Report 1170*, Lewis Flight Propulsion Laboratory, Cleveland, OH, 1954.



APPENDIX A  
FIGURES

<u>Figure No.</u>	<u>Title</u>	<u>Page No.</u>
A-1	Low Cycle Fatigue Test Specimens.....	12
A-2	Hydraulic Impulse Fatigue Test Specimen	
	(a) Overall View .....	13
	(b) PD Measurement Wiring Soldered on Specimen.....	14
A-3	Hydraulic Impulse Fatigue Test Fixture .....	15
A-4	Pressure Waveform of SAE ARP 603 .....	16
A-5	Micrographs of Tube and Rod .....	17
A-6	Crack Surface of Tube Specimen, Subjected to.....	18
	Hydraulic Impulse Fatigue and Heat-Tinting	
A-7	Calibration Curve of $[(V/V_0) - 1]$ Versus Crack Depth <b>a</b> .....	19
A-8	Calibration Curve of $[(V/V_0) - 1]$ Versus Normalized Crack Depth <b>a/B</b> .....	20
A-9	Stable Hysteresis Loop .....	21
A-10	Shape Change of Hysteresis Loop with Strain-Cycle.....	22
A-11	Hysteresis Loop, Showing Elastic Moduli .....	23
A-12	Plot of Load Versus Strain Cycle .....	24
A-13	Plot of Modulus Ratio $Q_N$ Versus Strain Cycle $N$ .....	25
A-14	Fracture Surface of Tube, Showing Fatigue Crack Initiation Near $N_i$ .....	26
A-15	Strain-Life Curve .....	27
A-16	Strain-Life Curves for Fatigue Crack Initiation and.....	28
	50% Load Drop in Tube Specimen	
A-17	Strain-Life Curves for Fatigue Crack Initiation,.....	29
	50% Load Drop and Fracture in Rod Specimen	
A-18	Strain-Life Curves of Tube and Rod Specimens, .....	30
	Comparing Crack Initiation Reversals $2N_i$	
A-19	Strain-Life Curves of Tube and Rod Specimens, .....	31
	Comparing 50% Load Drop Reversals $2N_{50}$	

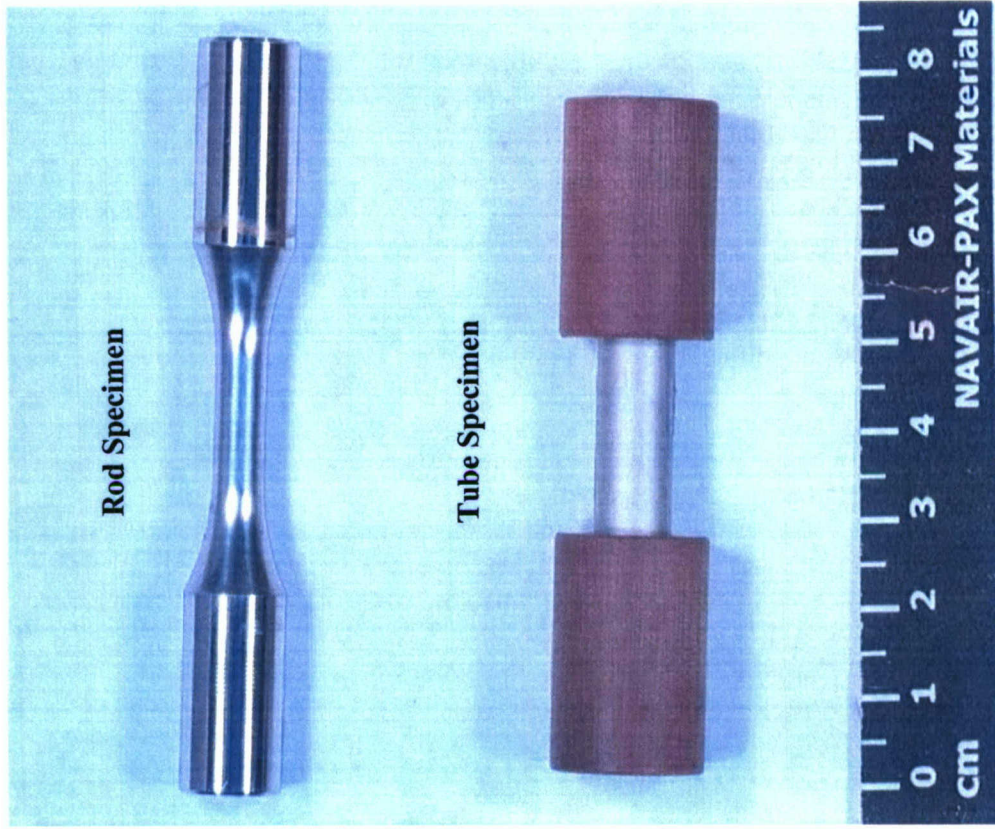


Figure A-1: Low Cycle Fatigue Test Specimens

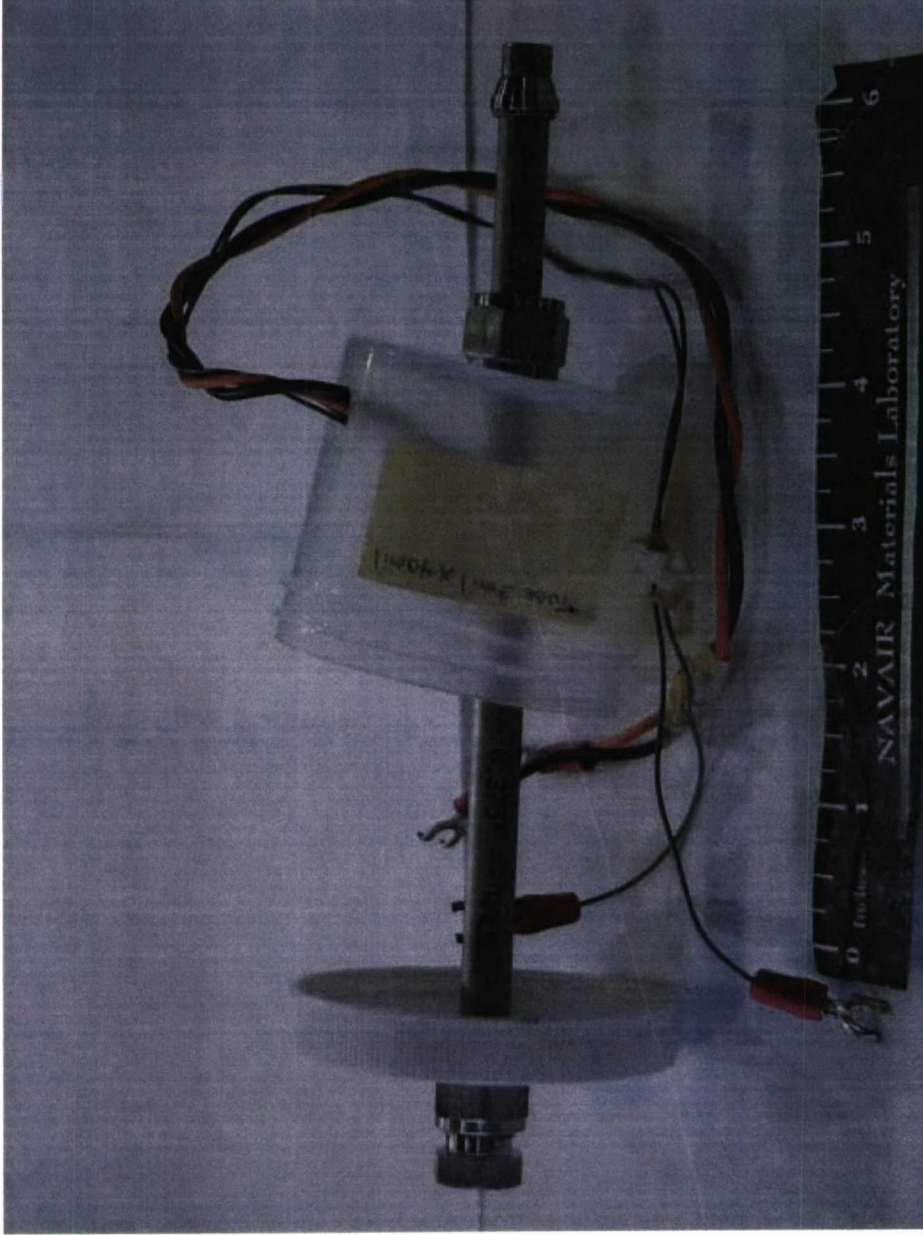


Figure A-2: Hydraulic Impulse Fatigue Test Specimen  
(a) Overall View

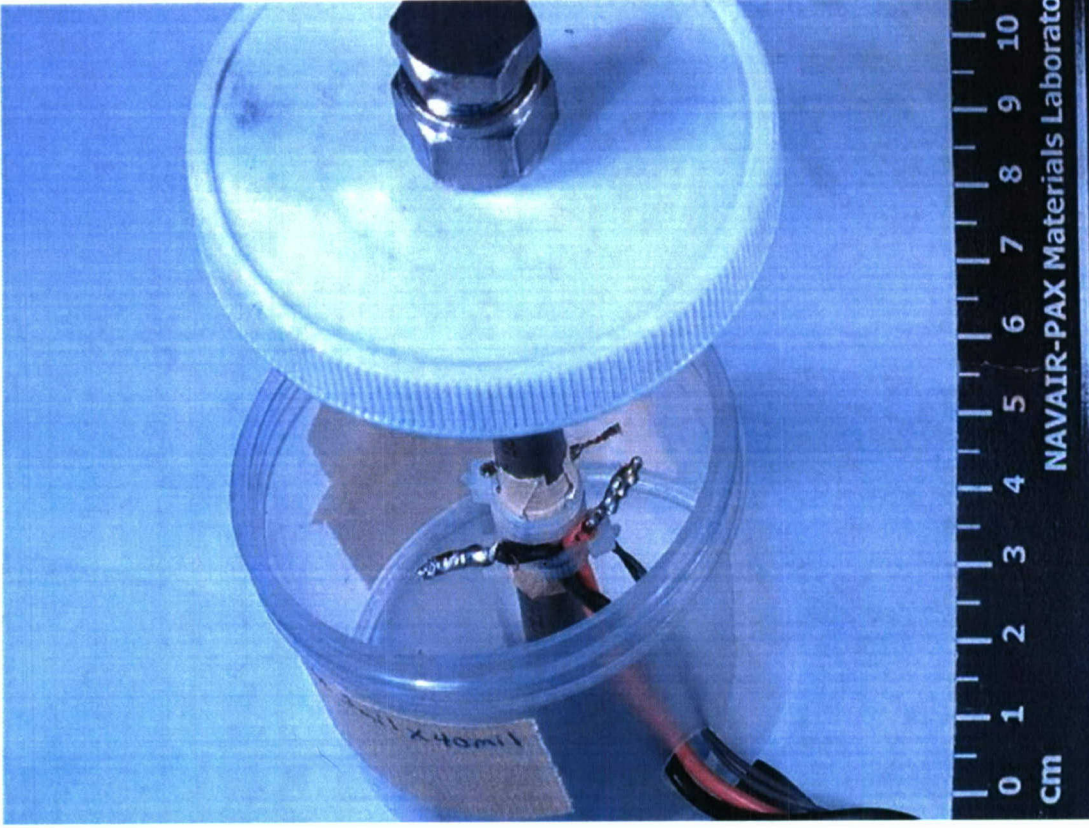


Figure A-2: Hydraulic Impulse Fatigue Test Specimen  
(b) PD Measurement Wiring Soldered on Specimen

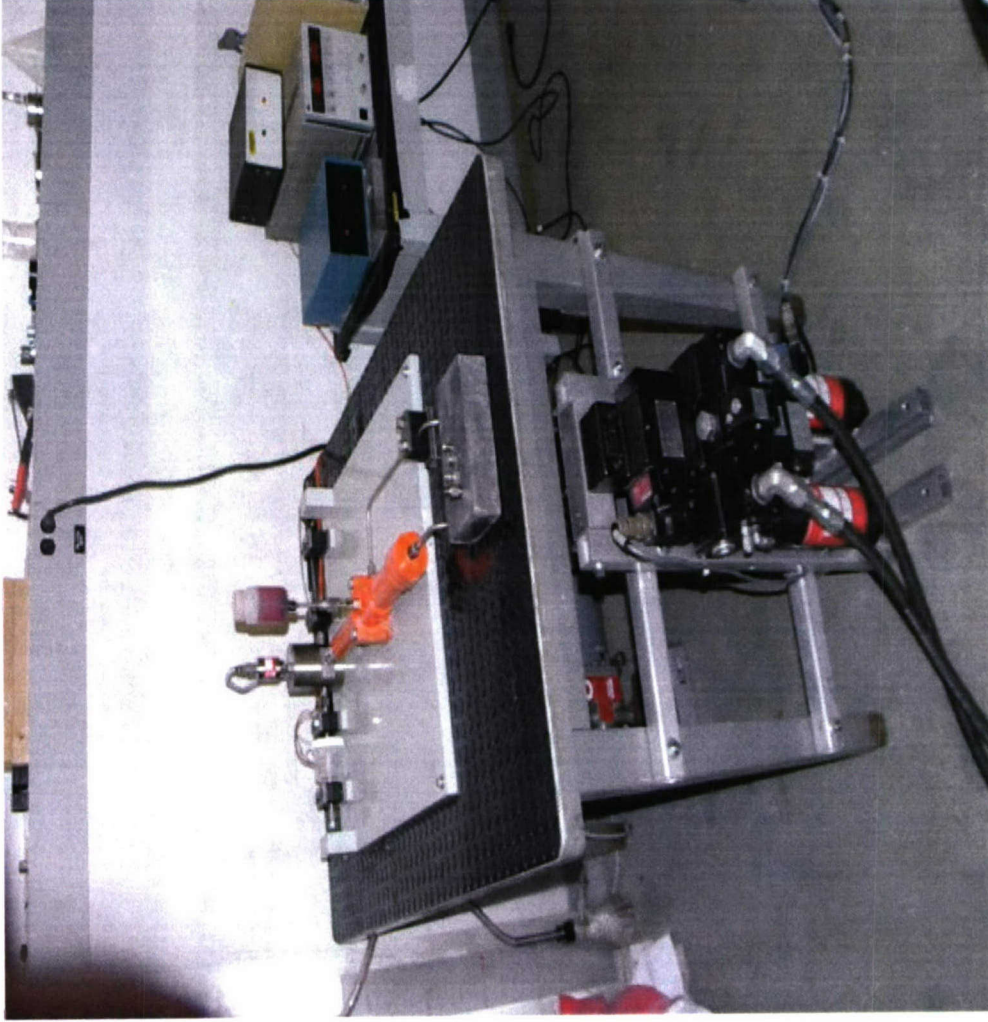


Figure A-3: Hydraulic Impulse Fatigue Test Fixture

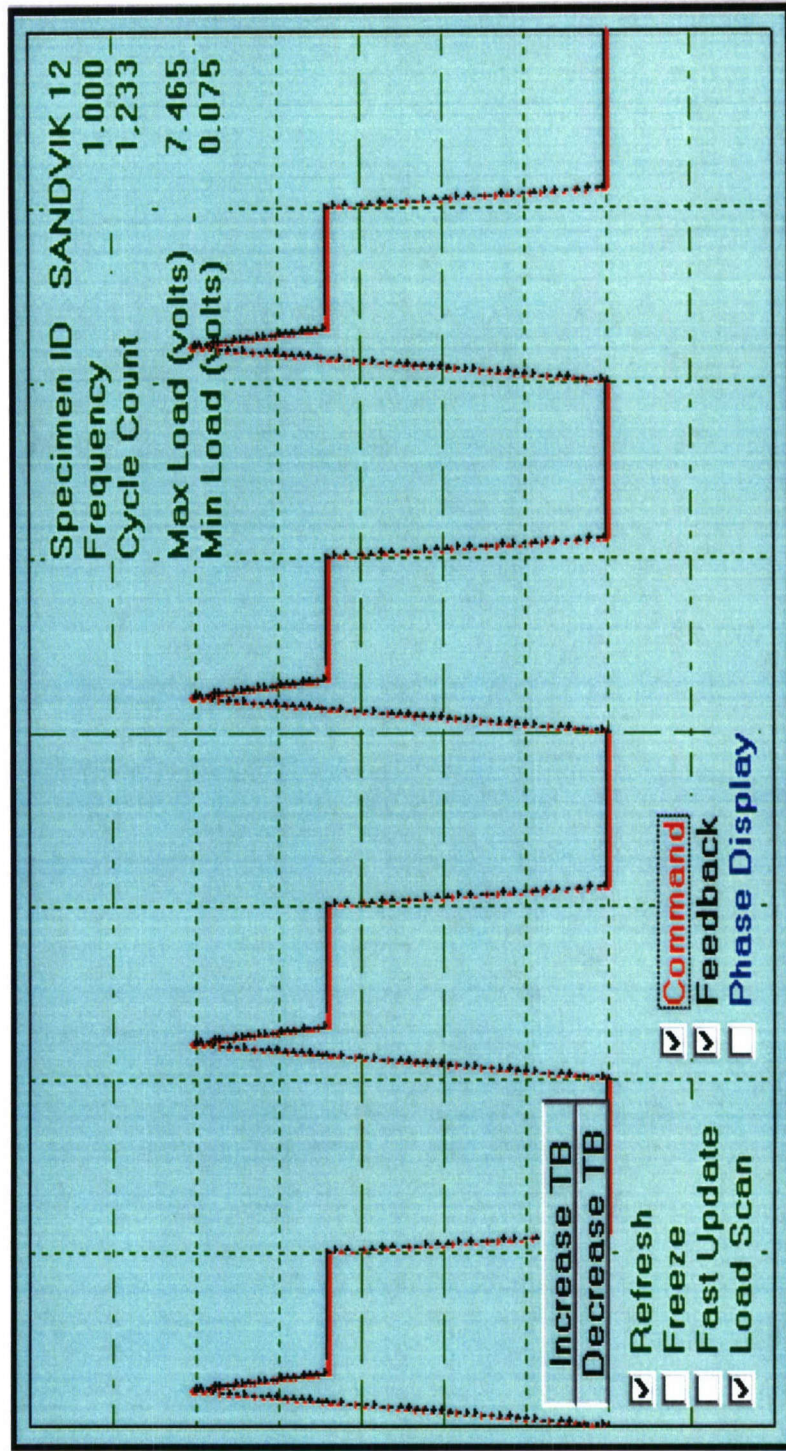
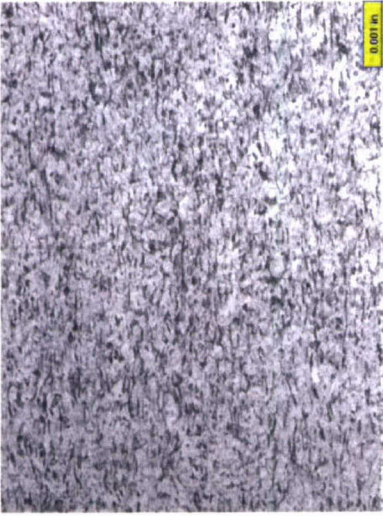


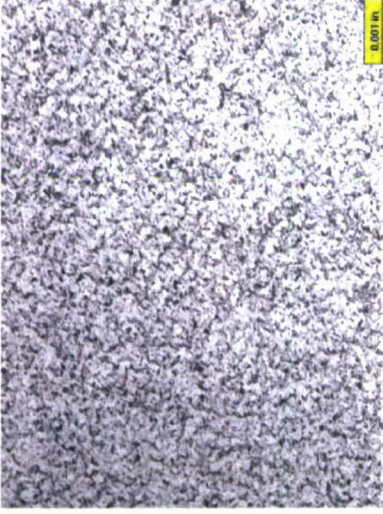
Figure A-4: Pressure Waveform of SAE ARP 603

**Tube**

**Longitudinal Face**



**Cross-Section**



**Rod**

**Longitudinal Face**



**Cross-Section**

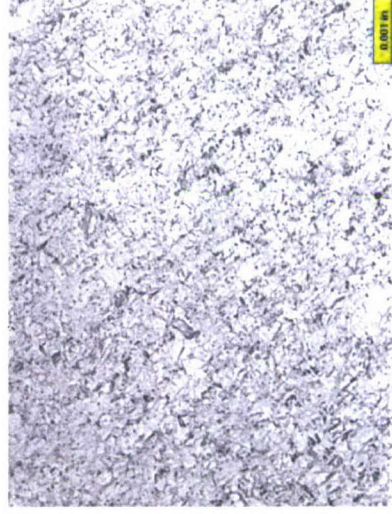
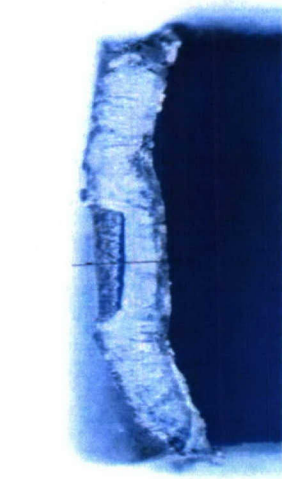


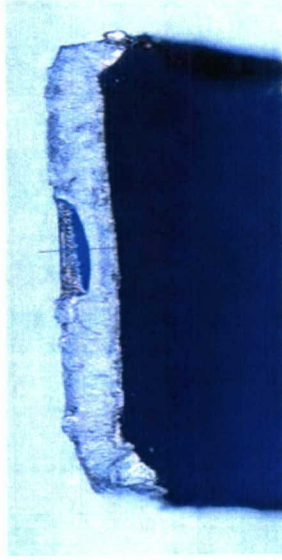
Figure A-5: Micrographs of Tube and Rod



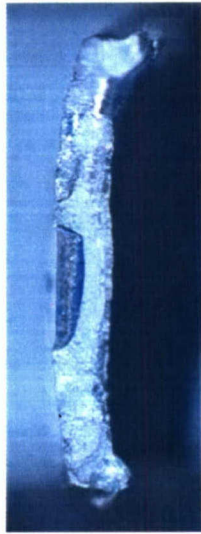
**1,261 cycles**



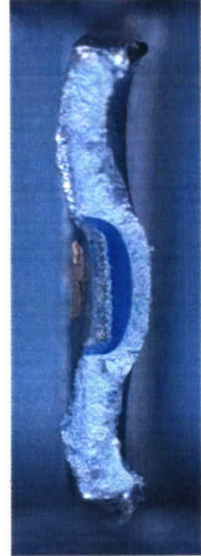
**3,761 cycles**



**3,981 cycles**



**4,508 cycles**



**8,065 cycles**



**9,071 cycles**



**11,056 cycles**

Figure A-6: Crack Surface of Tube Specimen, Subjected to Hydraulic Impulse Fatigue and Heat-Tinting



### Calibration Curve

$V_o$ : initial PD

V: PD at N cycle

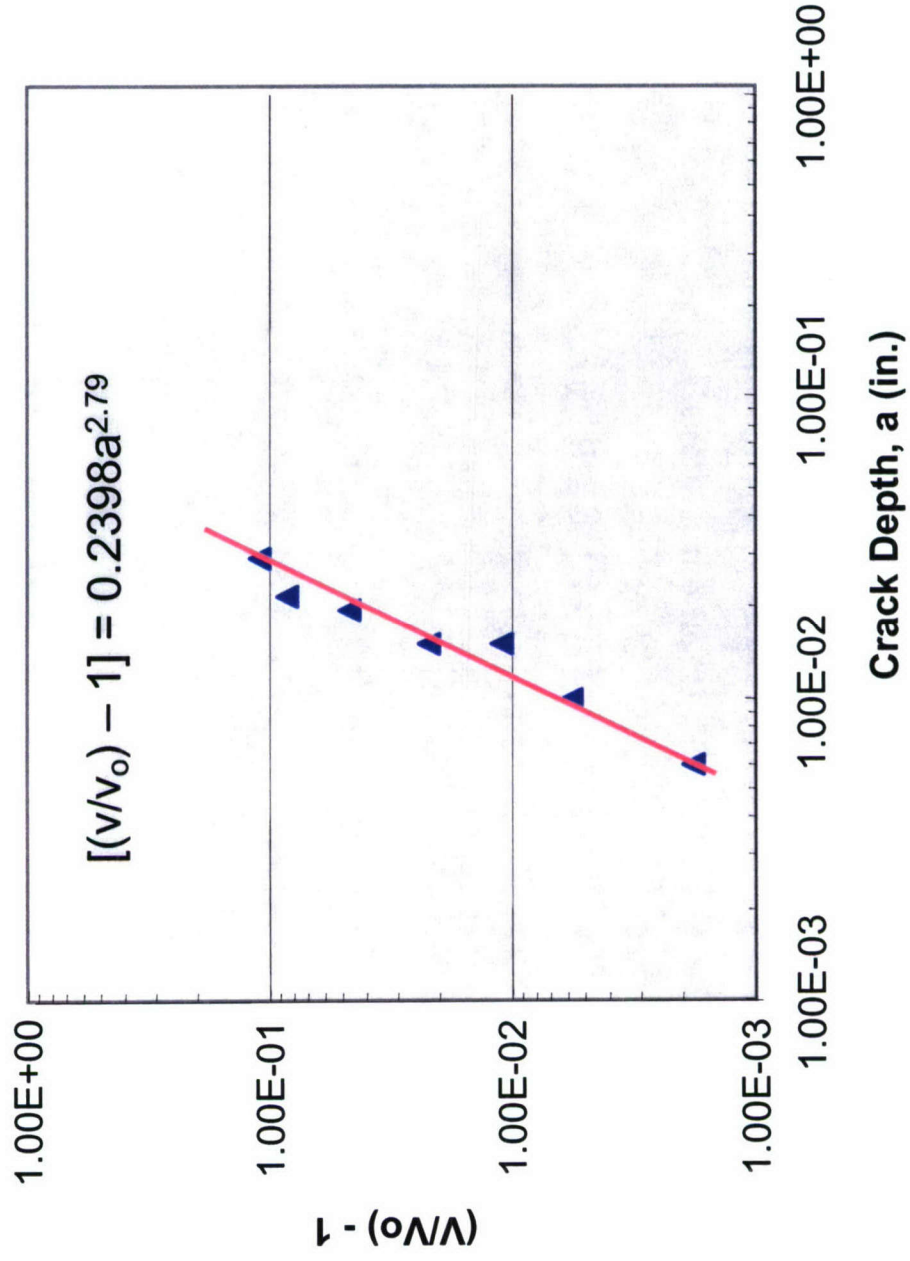


Figure A-7: Calibration Curve of  $[(V/V_o) - 1]$  Versus Crack Depth a

### Calibration Curve

$V_0$ : initial PD

$V$ : PD at N cycle

$B$ : tube thickness

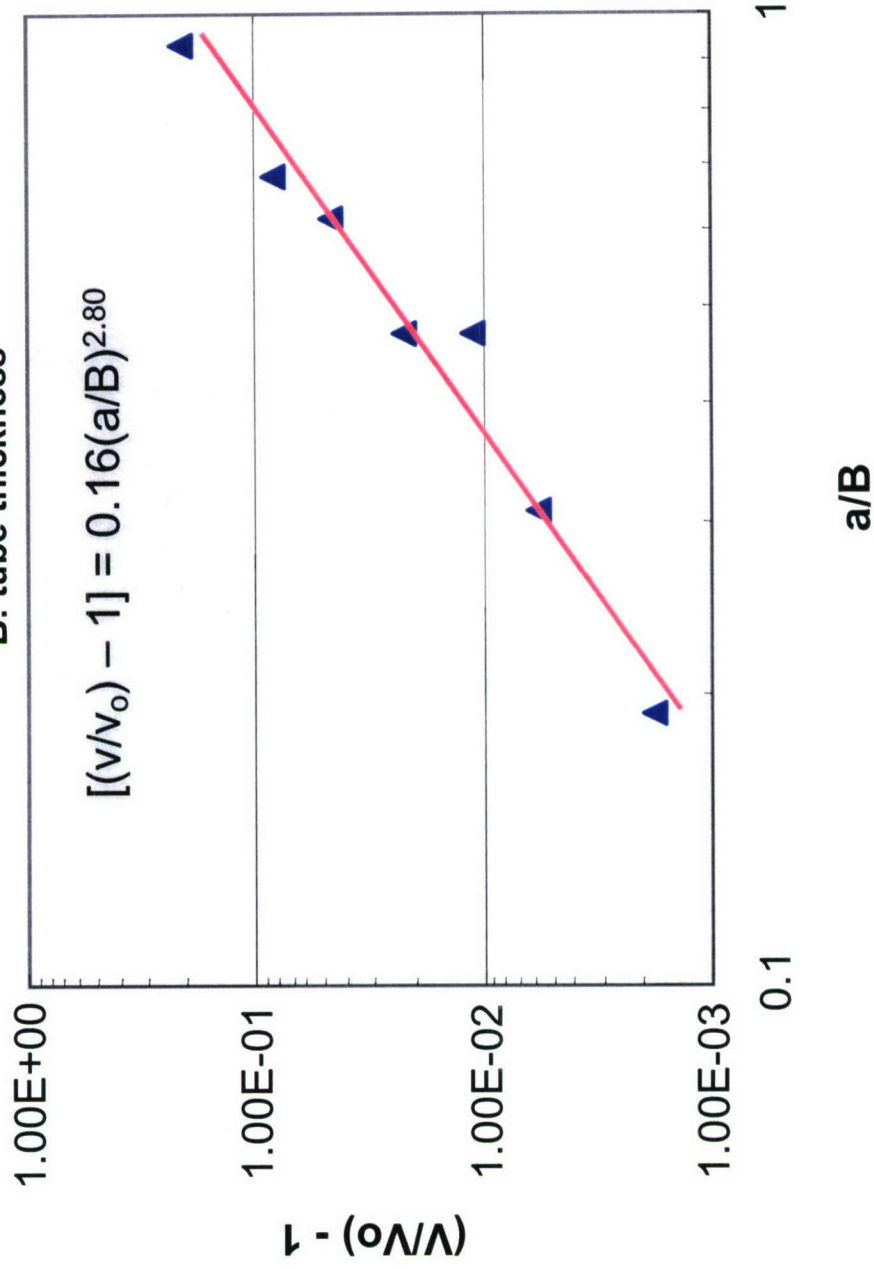
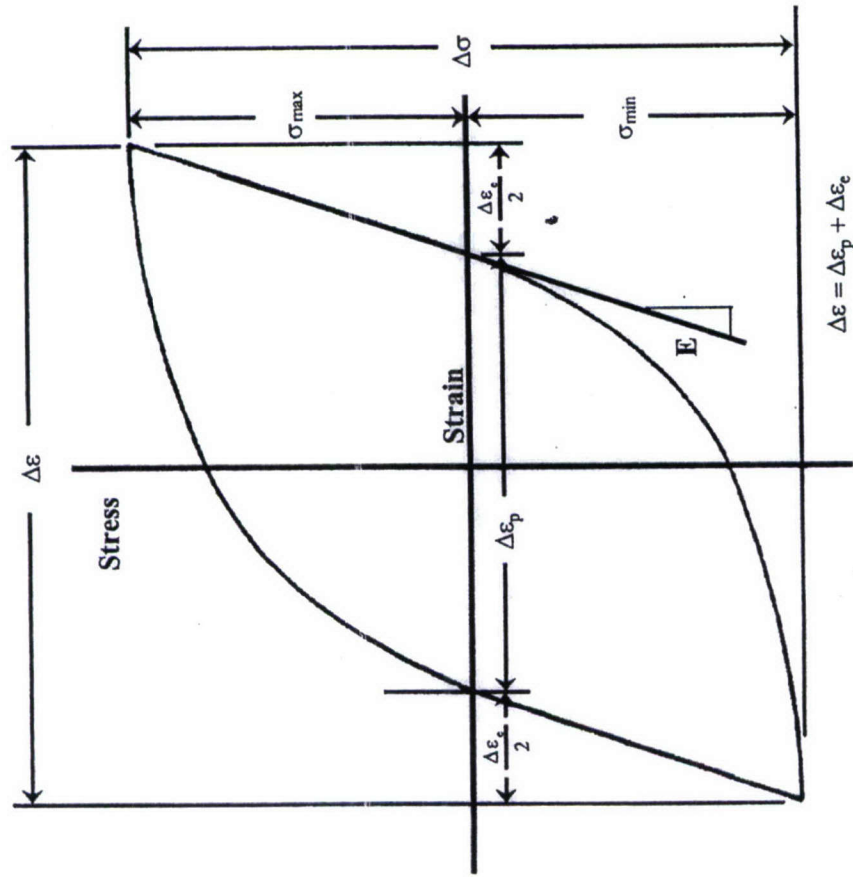
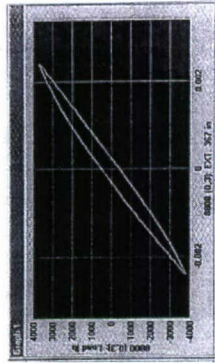


Figure A-8: Calibration Curve of  $[(V/V_0) - 1]$  Versus Normalized Crack Depth  $a/B$

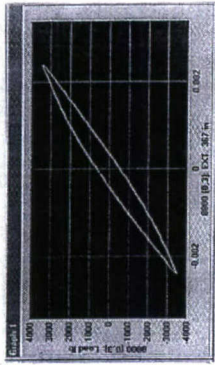


Stable Hysteresis Loop

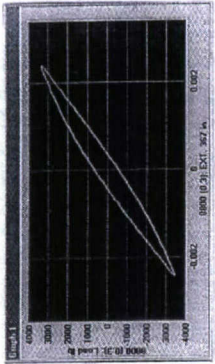
Figure A-9: Stable Hysteresis Loop



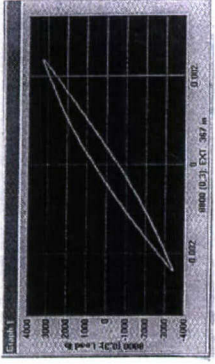
**N= 36**



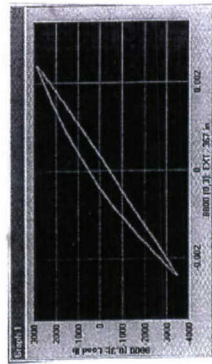
**N= 735**



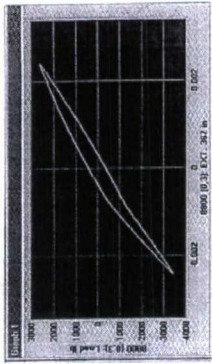
**N= 1630**



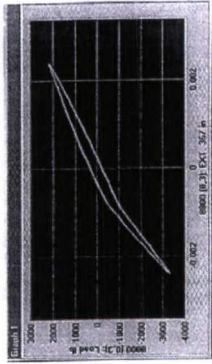
**N= 3960**



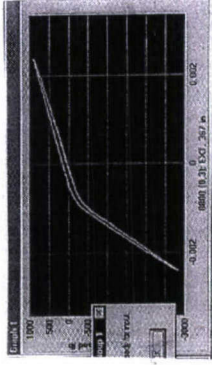
**N= 4607**



**N= 4816**

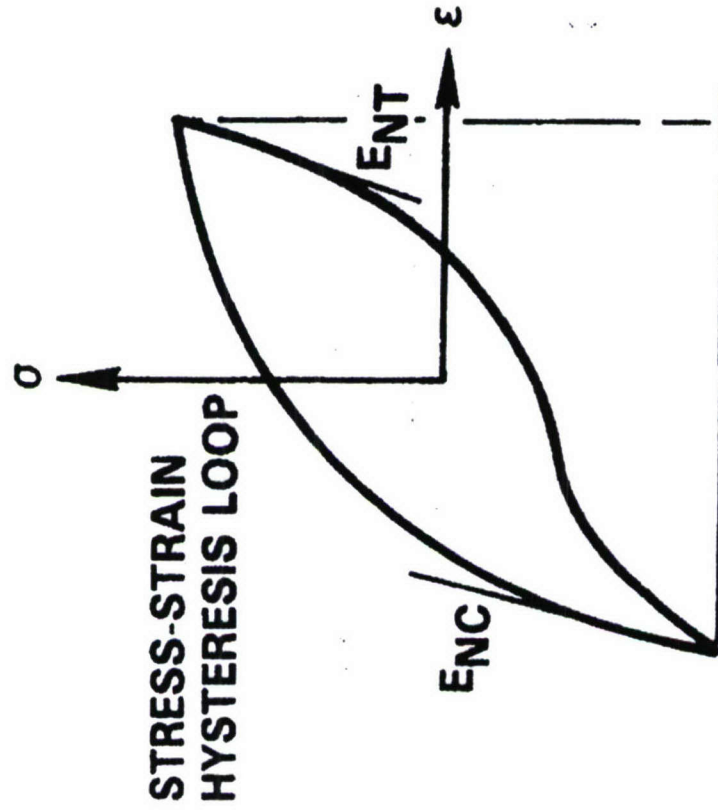


**N= 5004**



**N= 5771**

Figure A-10: Shape Change of Hysteresis Loop with Strain-Cycle



$$Q_N = E_{NT}/E_{NC}$$

Figure A-11: Hysteresis Loop, Showing Elastic Moduli

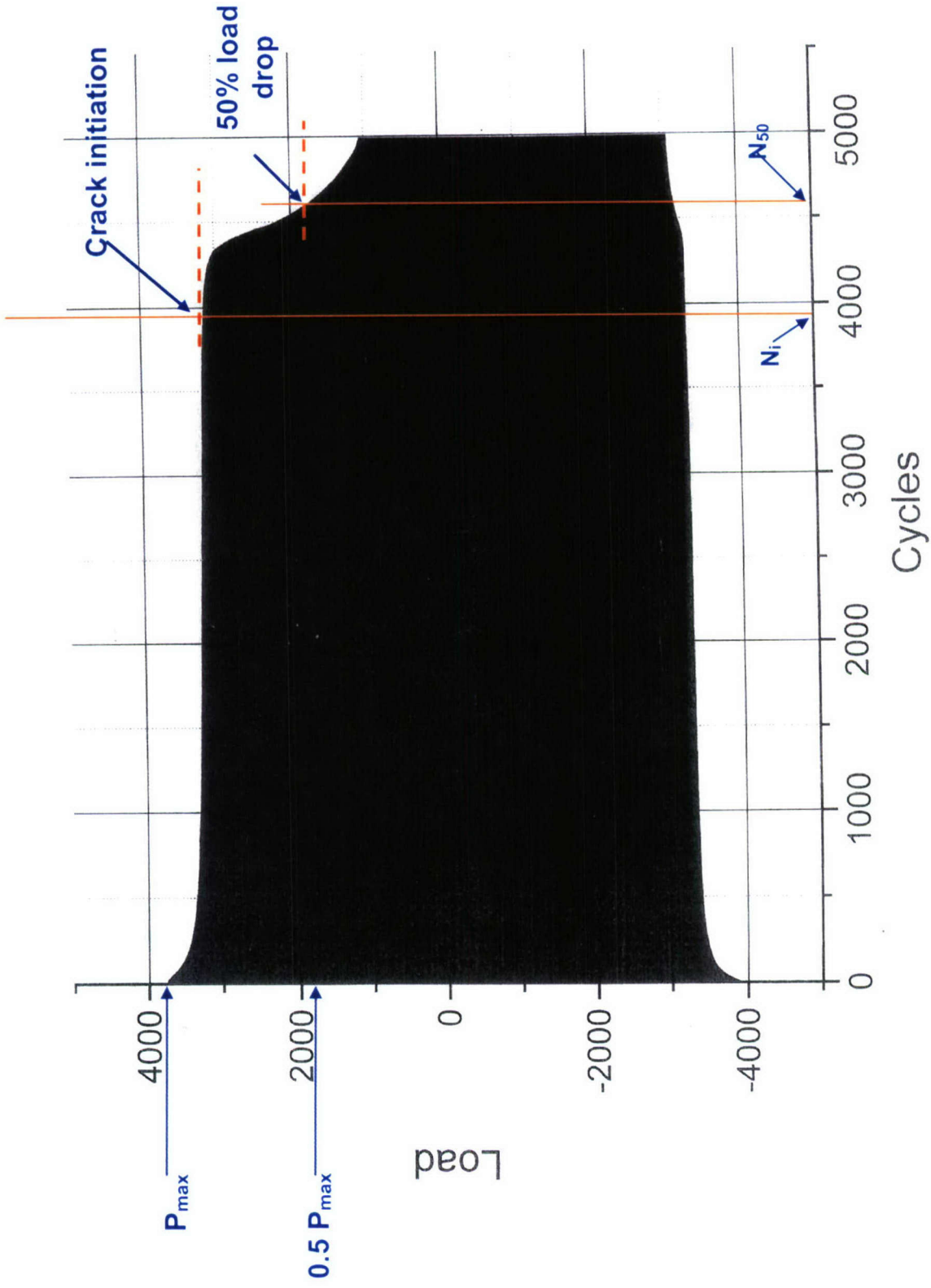


Figure A-12: Plot of Load Versus Strain Cycle

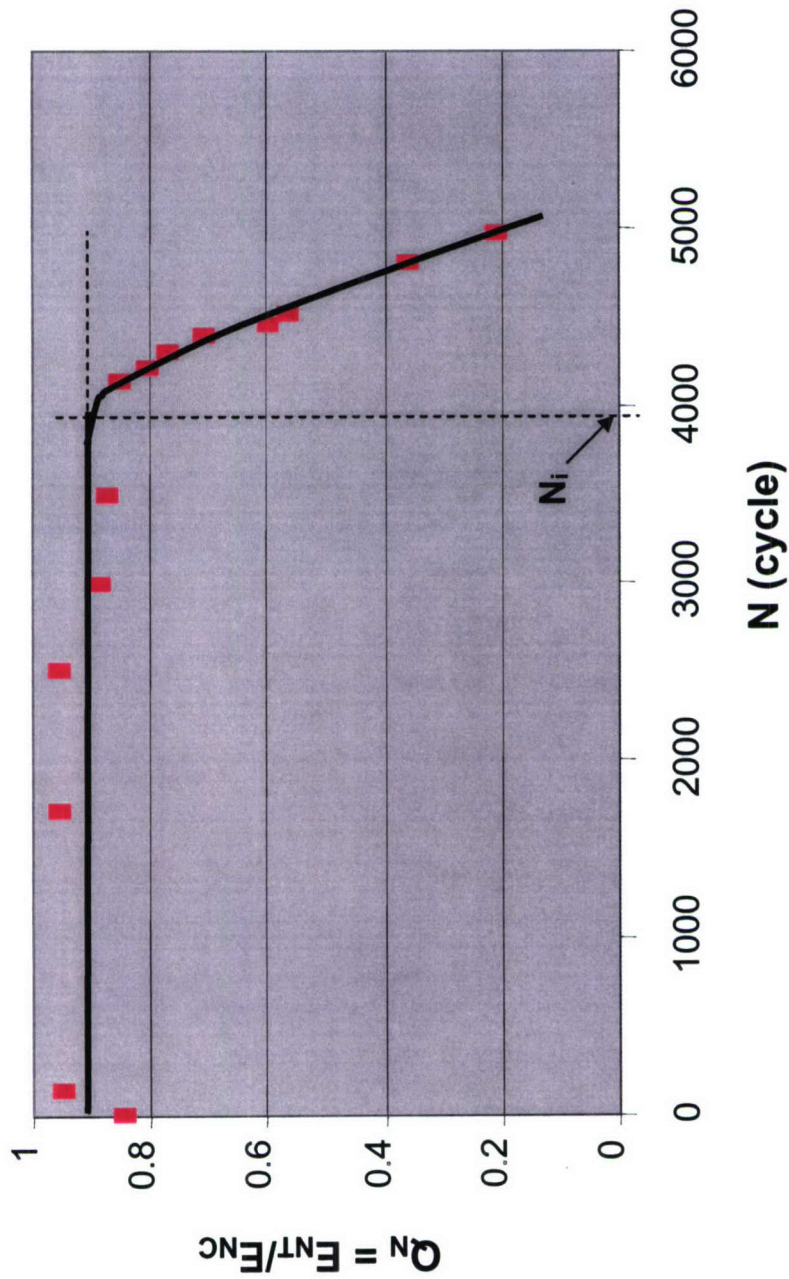


Figure A-13: Plot of Modulus Ratio  $Q_N$  Versus Strain Cycle N

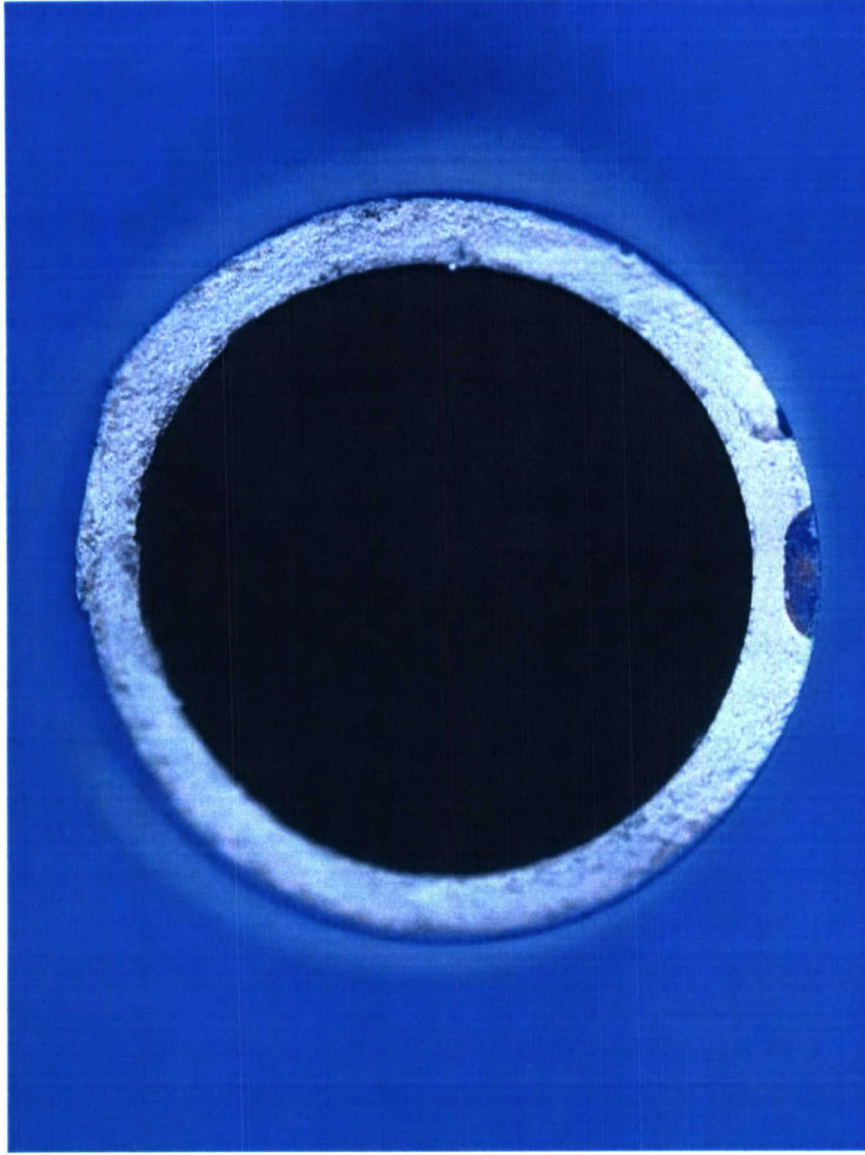


Figure A-14: Fracture Surface of Tube, Showing Fatigue Crack Initiation Near  $N_i$



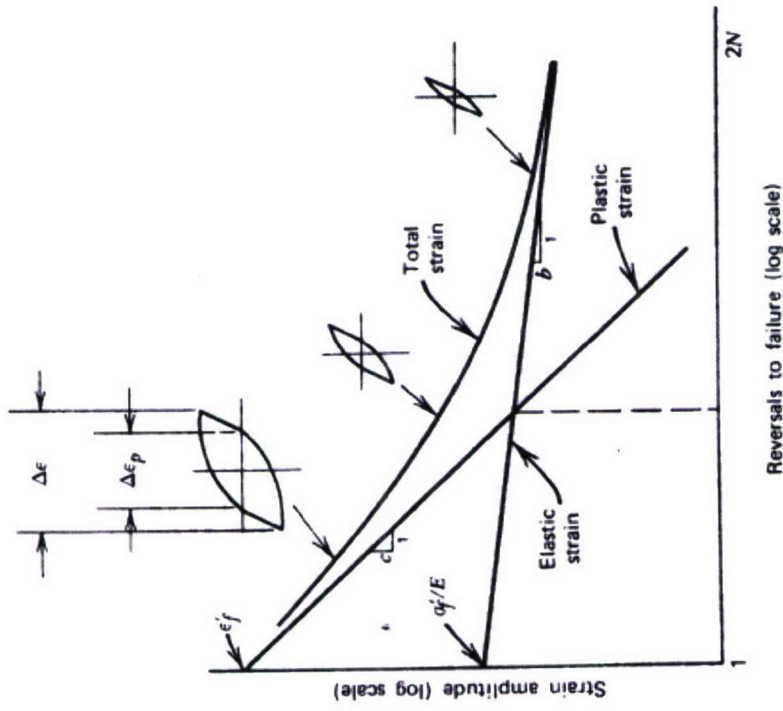


Figure A-15: Strain-Life Curve

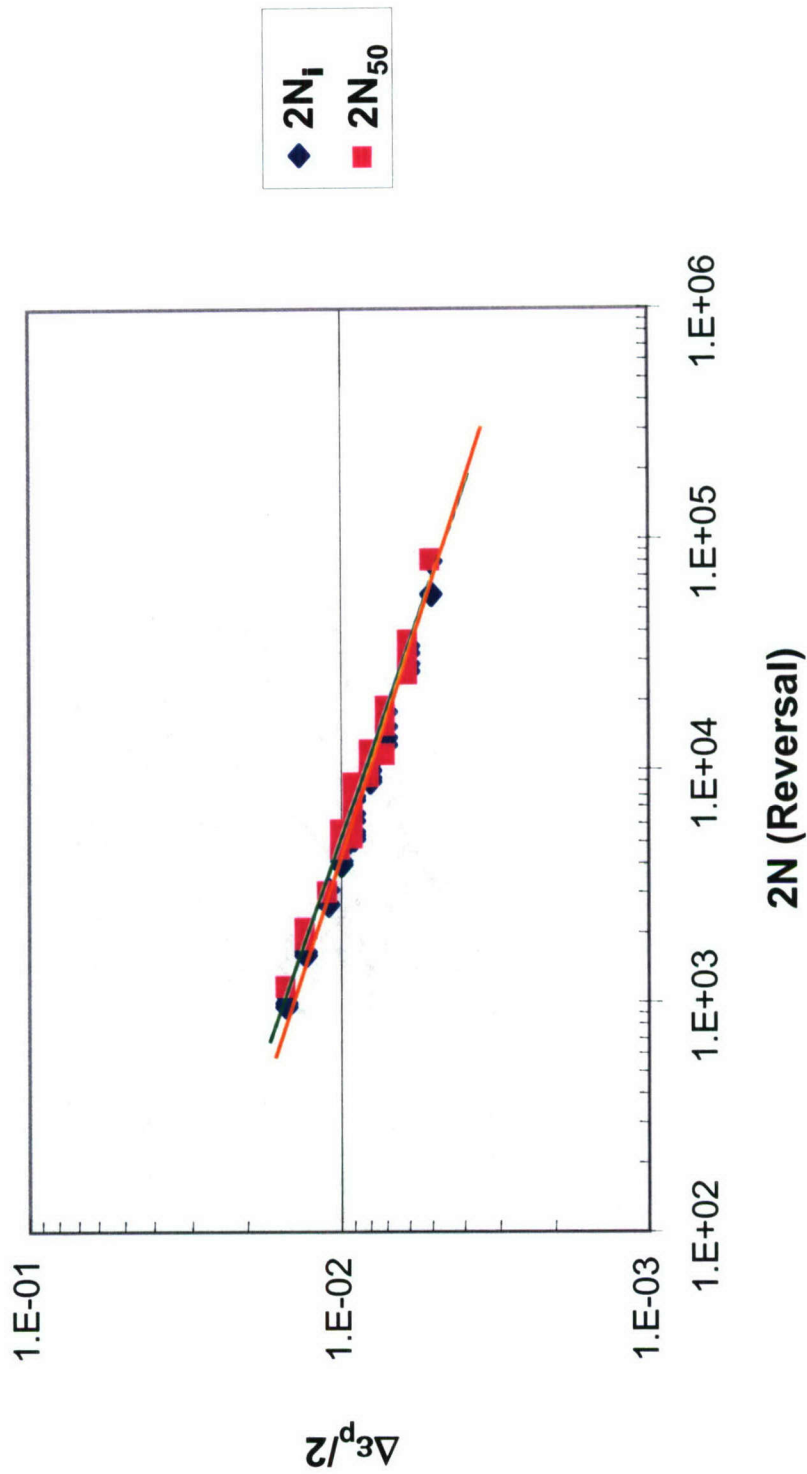


Figure A-16: Strain-Life Curves for Fatigue Crack Initiation and 50% Load Drop in Tube Specimen

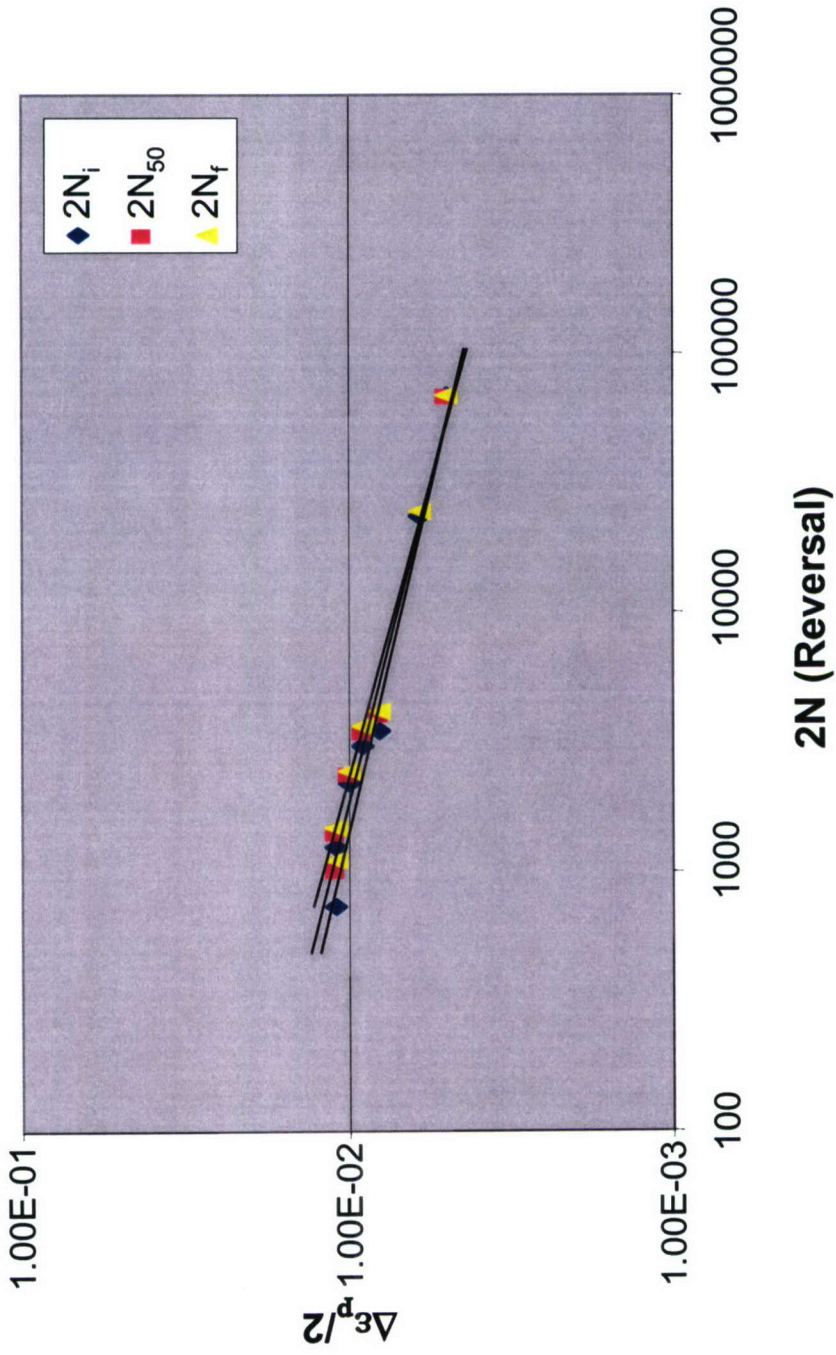


Figure A-17: Strain-Life Curves for Fatigue Crack Initiation, 50% Load Drop and Fracture in Rod Specimen

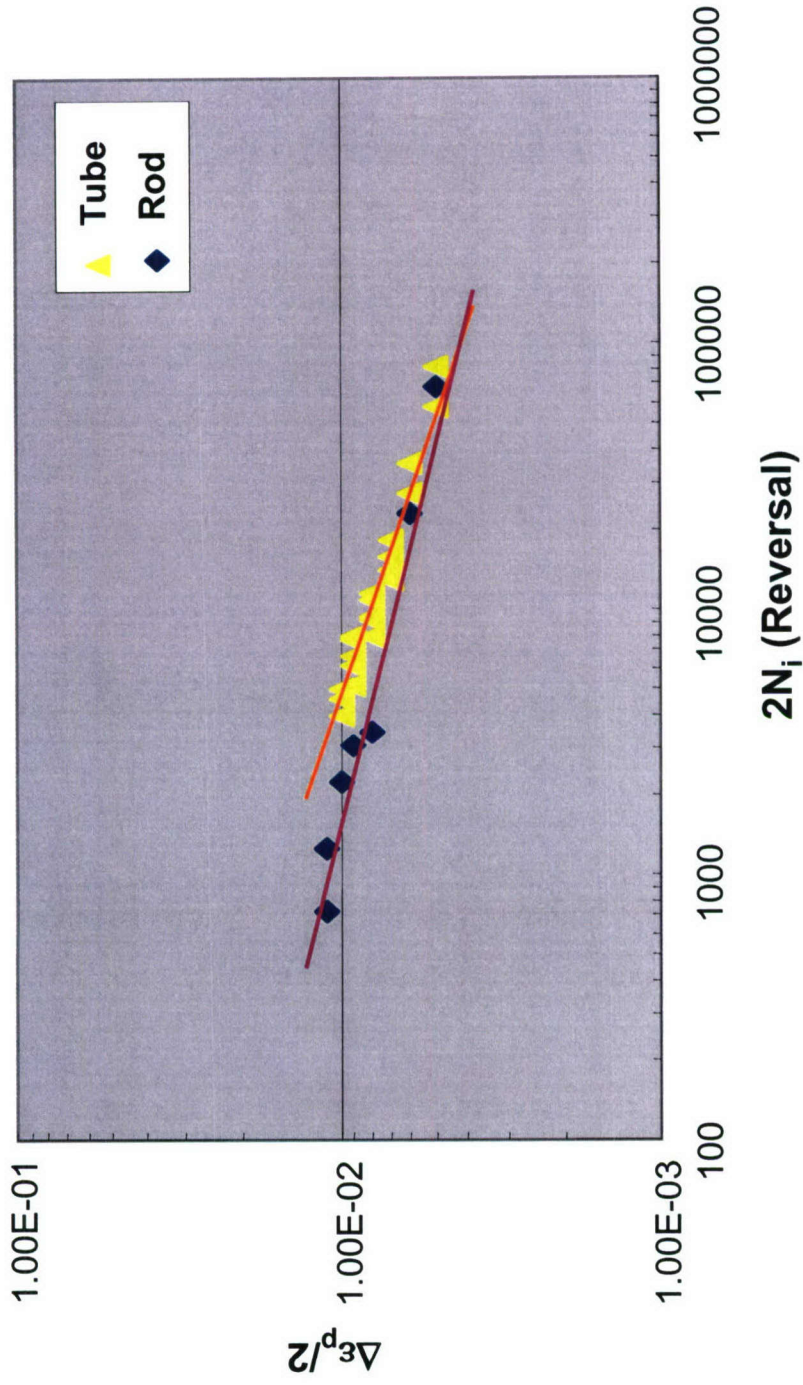


Figure A-18: Strain-Life Curves of Tube and Rod Specimens, Comparing Crack Initiation Reversals  $2N_i$

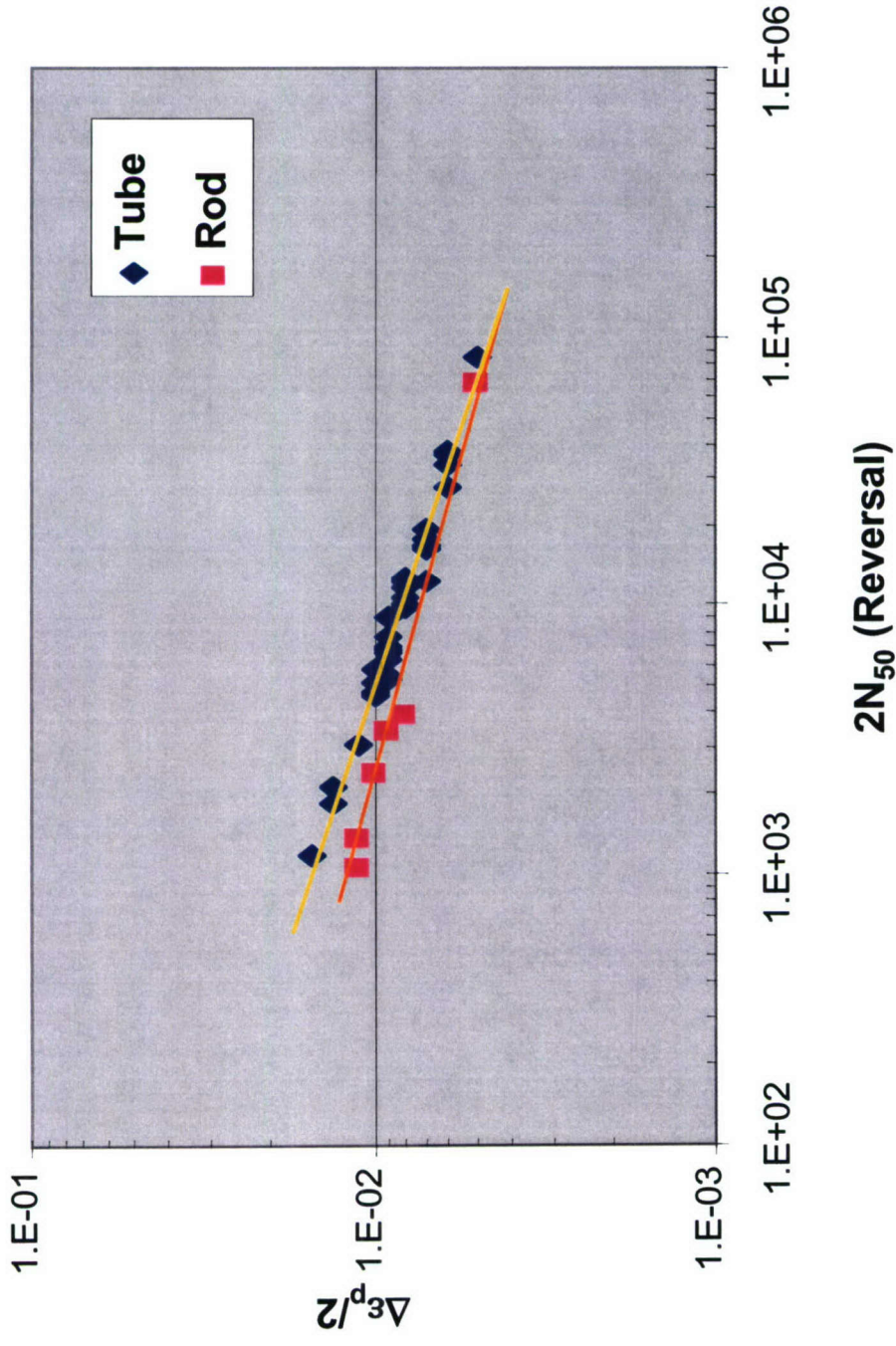


Figure A-19: Strain-Life Curves of Tube and Rod Specimens, Comparing 50% Load Drop Reversals  $2N_{50}$

DISTRIBUTION:

NAVAIRSYSCOM (AIR-4.3), Bldg. 2187, Room 3371 (1)  
48110 Shaw Road, Patuxent River, MD 20670-1906

NAVAIRSYSCOM (AIR-4.3.4), Bldg. 2188, Room 203G (1)  
48066 Shaw Road, Patuxent River, MD 20670-1908

NAVAIRSYSCOM (AIR-4.0X), Bldg. 407, Room 116 (1)  
22269 Cedar Point Road, Patuxent River, MD 20670-1120

NAVAIRSYSCOM (AIR-5.1), Bldg. 304, Room 100 (1)  
22541 Millstone Road, Patuxent River, MD 20670-1606

NAVAIRWARCENACDIV (4.3.4.1), Bldg. 2188, Room 203C (20)  
48066 Shaw Road, Patuxent River, MD 20670-1908

NAVTESTWINGLANT (55TW01A), Bldg. 304, Room 200 (1)  
22541 Millstone Road, Patuxent River, MD 20670-1606

Army Materials Command (AMCCE-BD) (1)  
5001 Eisenhower Ave., Alexandria, VA 22333

NAVSEASYSYSCOM (1)  
2531 Jefferson Davis Highway, Arlington, VA 22242

Naval Research Laboratory (1)  
4555 Overlook Ave. S. W., Washington, DC 20375-5000

NADEP (AIR-4.3.4) (1)  
Naval Air Station, Jacksonville, FL 32212

NADEP (AIR-4.3.4) (1)  
PO Box 377058, San Diego, CA 92135-5112

NADEP (AIR-4.3.4) (1)  
PSC Box 8021, Cherry Point, NC 28533-0021

NAWCWD (1)  
1 Administration Circle, China Lake, CA 93555-6001

NAVAIRWARCENACDIV (1)  
Highway 547, Lakehurst, NJ 08733-5100

Office of Naval Research (1)  
875 N. Randolph St., Arlington, VA 22203-1995

DTIC (1)  
8725 John J. Kingman Road, Suite 0944, Ft. Belvoir, VA 22060-6218

**UNCLASSIFIED**

**UNCLASSIFIED**